

Monitoring of Tidal Variations of the Underground Water Level in a Group of Water-bearing Horizons

A. A. Lyubushin, Jr., V. A. Malugin, and O. S. Kazantseva

*Institute of Experimental Geophysics, Schmidt Joint Institute of Physics of the Earth,
Russian Academy of Sciences, Moscow, Russia*

Received September 26, 1994

Abstract—Synchronous observations in the Moscow region of the underground water level in four holes to the depths of water-bearing horizons (120, 180, 400, and 1000 m) are analyzed. Prominence is given to tidal variations of the level in a moving time window with the goal of revealing local and regional anomalies in the state of the geophysical medium. The study includes cross-spectrum analysis of each of the levels and theoretical tidal volume deformation, as well as multidimensional combined analysis of all the levels. The method described may be used for identification of the most significant water-bearing horizons.

INTRODUCTION

Variations in the formation pressure of the water-bearing horizons are the most significant geophysical characteristics indicating the state of the upper crust. This is related with the fact that the water-bearing beds are in fact vast volume strainmeters accumulating and averaging strains over appreciable parts of the crust. We are interested in the part of the formation pressure caused by deformation variation (such as seasonal, lunar–solar tidal, anthropogenic, atmospheric and other deformations) in water-containing rocks.

This paper continues the previous one [1], where variations in the underground water level relative to baric variations were studied. By estimating the evolution of the amplitude frequency transfer function of pressure variation toward the level in the moving time window, the nonstationary effect of strength of the upper crust was revealed, and the hypothesis of origination of this nonstationarity was offered [1]. The hypothesis is the superposition of spatial patchiness of high-frequency pulsations of the atmospheric pressure (with periods of less than 10 h) on the block nonuniformity of the crust in the vicinity of the hole. In fact, the natural baric variations were used by Lyubushin and Malugin [1] as a sounding signal enabling them to estimate change in the properties of the medium. However, in this paper, we use the tidal variations in the formation pressure as a sounding signal [2].

The study of tidal response of the underground water level and identification of tidal harmonics in variations of the level are the traditional topic of hydrodynamic investigations [3–8]. The tidal response was studied mainly on the basis of the assumption of stationary properties of the medium. Sardarov and Ali-

bekov [7] considered variability of the tidal variations in the concentration of gas. Kissin and Gumen [8] studied the time variability of the amplitude and phase of the M_2 harmonic in the level variations from observations in a region with intense creep movements (Pripyatskaya basin). Applied to the analysis of the measured level in seismic regions, the hypothesis that change in the “rhythm” of tidal variations in the level may serve as a prognostic indicator of earthquakes was proposed. In this connection, the question of the extent of the tidal rhythms of the level variations in aseismic platform regions (Moscow region) for different water-bearing horizons and the question of the relation between the variable rhythms of different horizons are of especial interest. These questions are the topic of this paper.

INITIAL DATA

We deal with synchronous series of the level variations of underground water in four holes drilled down to the horizons at depths of 120, 180, 400, and 1000 m. Two of the four holes (to depths of 120 and 180 m) are located in Zelenyi settlement, Moscow region (Noginsk area, east of Moscow), and the other two are northwest of Moscow, at the territory of the Central Institute of Traumatology and Orthopedics (CITO). Thus, we have the two sites of observations spaced at a distance of about 40 km, and, at each of the sites, the level and atmospheric pressure variations are recorded in digital form (in blocks of solid-state memory with subsequent rewriting in the hard disc of a PC) at the discretization interval of $\Delta t = 10$ min. Before processing, the series were averaged and thinned out 6 times, so that the dis-

Characteristics of holes and water-bearing horizons

No.	Name of horizon, site of hole	Depth of filter, m	Thickness, m	Additional information
1	Nizhnegzhel'skii, Zelenyi settlement	98–122	20–30	Intense water supply
2	Myachkovsko-podol'skii, Zelenyi settlement	137–183	50–70	Used for water supply
3	Verkhnefamenskii, Moscow (CITO)	368–399	≈200	Not used for supply
4	Nizhneshchigrovskii, Moscow (CITO)	904–1013	80–100	Lenslike occurrence, no water supply

cretization interval increased to 1 h. The sensitivity of the transducers of the primary data is 0.1 mm of water column for the level and 10 microbars for the pressure. Synchronous observations started at the two sites on February 2, 1993, at 12 : 10 local time; the duration of the processed interval of observations is 9887 h (up to March 17, 1994). In the Zelenyi settlement, observations started much earlier, on October 23, 1991 [1]. The table lists characteristics of the horizons [9].

The area of the occurrence of the horizons is wide, of the typical linear dimension of a few hundreds of kilometers, and covered the Moscow region and its vicinities [9]. Below, for brevity, we use the terms "horizon 120," "level 400," etc., meaning identification of the hole and water-bearing bed from the rounded lower depth of the filter. Note that water from horizons 120 and 180 (nos. 1 and 2, see table) is pumped out for settlements of the Moscow region (the pumping from horizon 120 is particularly intense, and the hole itself is at a distance of 1.5 km from a site of water supply). Horizons 400 and 1000 (nos. 3 and 4) are not used, and the holes at the CITO territory were drilled in the search for medical mineral water and have not been exploited for a few years. It must be noted that horizon 400 has a large thickness—2–7 times thicker than the other horizons.

Figure 1 shows the initial levels and the levels compensated for the atmospheric pressure effect (graphs of the compensated levels are shifted downward). The level is the height of the water column above the manometric sensor that is lowered into the hole. For compensating, an algorithm [10, 11] with a 2000-h adaptation window was used. Note the presence of the high-amplitude annual component (related to seasonal effects) for horizon 1000 (Fig. 1d). The component is of a regular character, the maximum level being in December–January, and the minimum level being in June–July.

Figure 2 presents the estimated power spectra of the compensated levels. It is seen that all of these contain the 12-h and 24-h peaks reflecting tidal variations. To a smaller extent, these peaks are pronounced for the deep horizon 1000 (Fig. 2d). Furthermore, an anomalous change in the slope of the graph for periods smaller than 16 h can be seen in the graph of the power spectrum for level 120. This anomaly was produced by the direct effect of water pumping (automatic turn-on and

off) for the supply of water from the horizon over a distance of 1.5 km.

Since our purpose is to analyze tidal variations in the water level, the question of their stability is of interest. For this, the compensated levels were passed through narrow-band filters with transmission bands of $(1/13, 1/11) \text{ h}^{-1}$ and $(1/27, 1/23) \text{ h}^{-1}$ for the 12- and 24-h tidal frequency bands, respectively. Then, the variance in the moving 48-h time window was calculated for each of the levels at the output of each of the two filters. Figure 3 shows variations in the variance for the 12-h tidal band for each of the levels and, for comparison, for the theoretical three-dimensional volume tidal deformation. Similar graphs for the 24-h tidal band are depicted in Fig. 4. The program for calculation of the tidal three-dimensional deformation (under the assumption of a spherical elastic earth model [2]) was courteously presented by V.L. Barabanov.

From the plots of variances for the 12-h tidal band (Fig. 3), we may preliminarily conclude that the theoretical tidal deformations (Fig. 3e) are most like the variations of level 400 (Fig. 3c), which, however, deviate at the moments of time $t \approx 3000$ and 5000 h. Level 120 (Fig. 3a) in the 12-h band is strongly disturbed by water pumping, and the trend observed is possibly caused by the increase in the water supply. It is difficult to distinguish intervals of agreement with the theoretically estimated volume deformation (these estimates are given below), but the anomaly of enhanced tidal variations in level 1000 for $t \approx 500$ – 1500 h is worthy of notice.

Similar conclusions may be reached in considering Fig. 4 (24-h tidal band), with the following differences: for level 400, to the intervals near $t \approx 3000$ and 5000 h of discrepancy between theoretical and observed tidal volume deformations, one may add those near $t \approx 7000$ h (Figs. 4c, 4d), and for level 120, the trend observed for the 12-h band disappeared (Fig. 4a).

METHOD OF PROCESSING

In processing the data, we pursue two goals: (1) to compare numerically tidal variations in each of the levels with theoretical tidal volume deformations; (2) to identify on the basis of the method of principal components frequency bands and time intervals in which tidal variations occur most synchronously in all the levels.

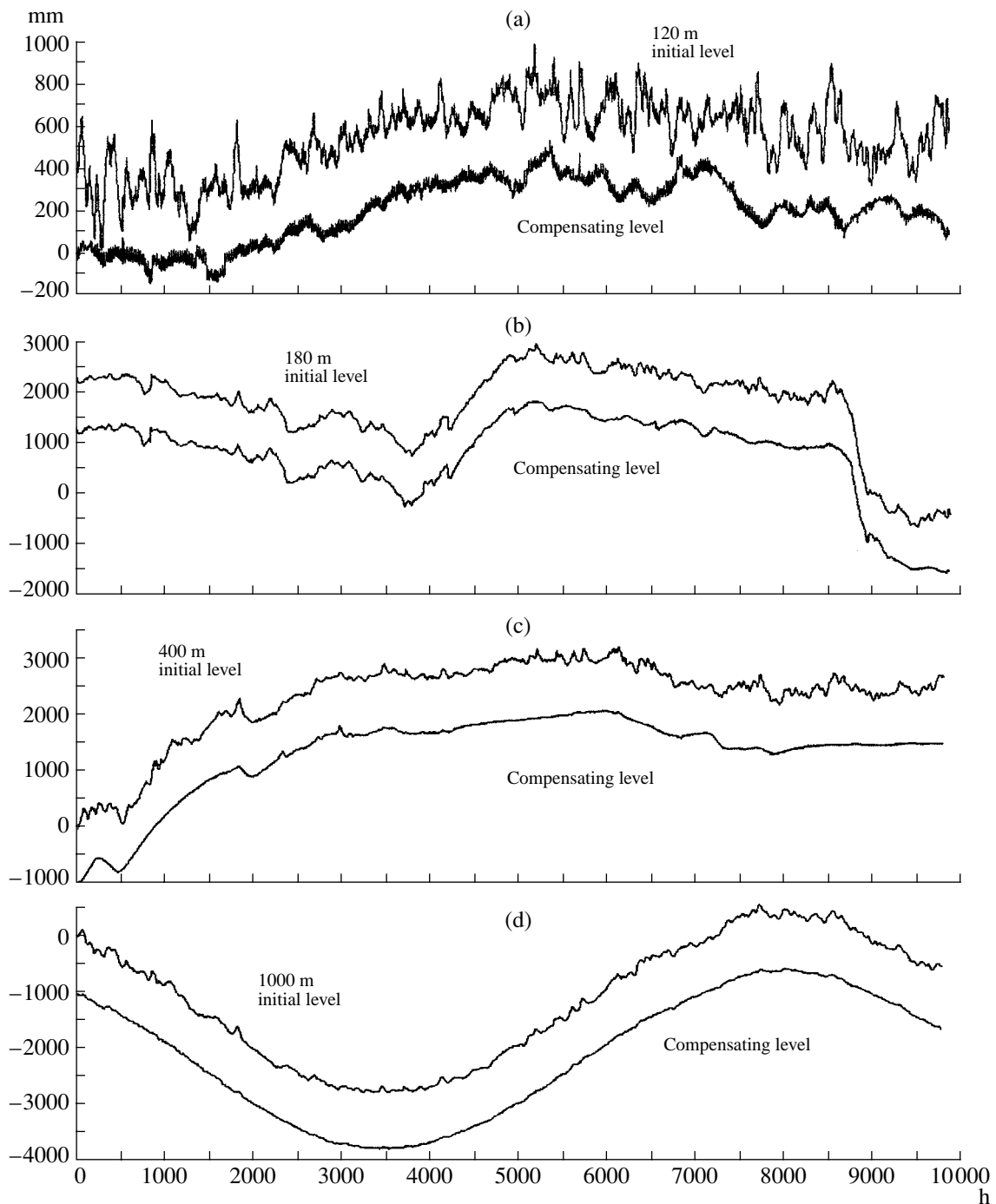


Fig. 1. Initial levels and levels compensated for atmospheric pressure (in heights of the water column above the transducer). The compensated levels are shifted downward.

The first of these problems is solved by estimating the evolution of the square of the coherence spectrum modulus γ^2 between variations in each of the levels and theoretical tidal variations in the moving time window. The method for solving the second problem, which extended the spectrum method of principal components to the nonstationary case, was described by Lyubushin [11, 12]. Its algorithm estimates the maximum eigen-

value of the spectrum matrix of the multidimensional series in the moving time window and visually shows the time–frequency dependence of the eigenvalue (as a function of frequency and the time coordinate of the window) in the form of level lines and volume surfaces. Examples of applying such a method in the search for seismic precursors in hydrogeochemical monitoring were given by Lyubushin [12]. Below we use the para-

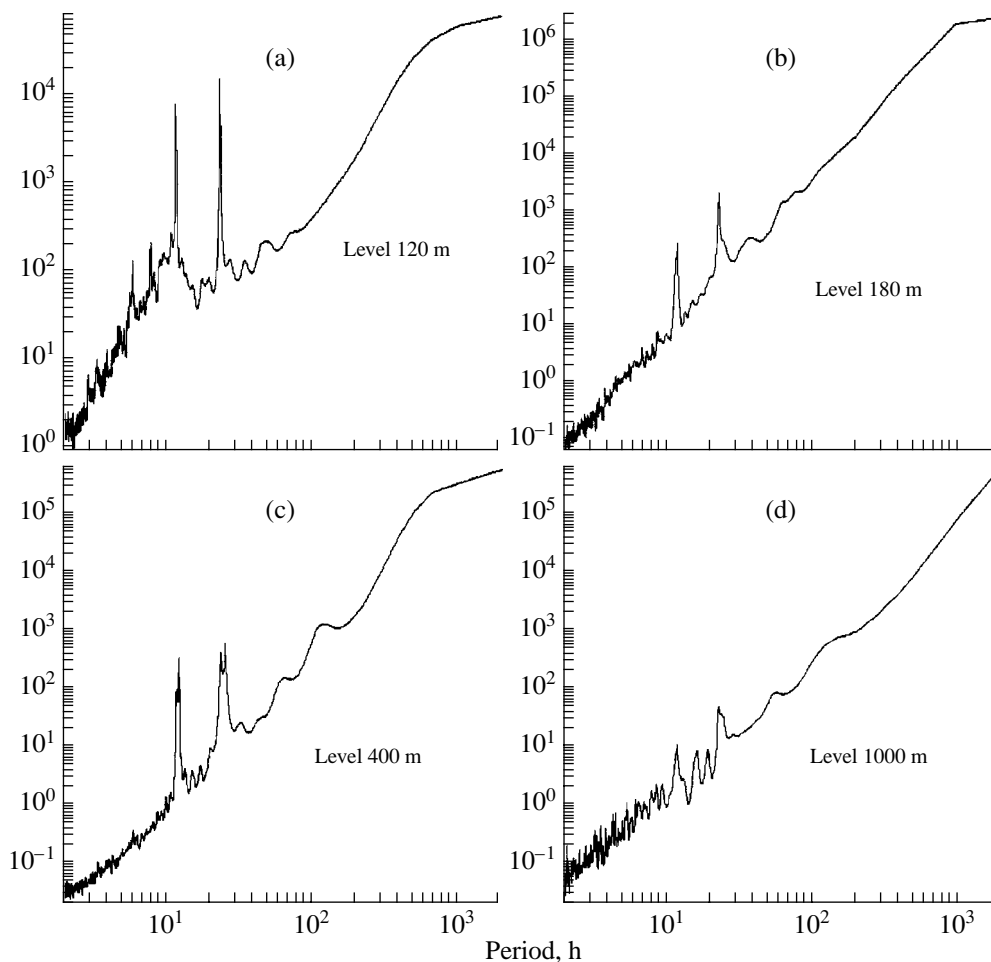


Fig. 2. Power spectra of compensated levels.

metric method for estimating the spectrum matrix, developed by Lyubushin [12] and based on the model of multidimensional autoregression [14]. The main points of this method are as follows.

Let $\mathbf{X}(t)$ be a vector time series to be analyzed; $\mathbf{X}(t) = (X_1(t), \dots, X_m(t))^T$, $X_i(t)$ be the scalar components of the multidimensional series, whose physical meaning and dimension may be different; T be the transposition sign; and t be the discrete time measured in Δt , units of discretization.

Since the time series to be analyzed are of low-frequency character (i.e., the power of the low-frequency components is substantially larger than that of the high-frequency components (Fig. 2)), we go over the series for the differences in order to remove the predominance of low frequencies; i.e., instead of $X_i(t)$, we consider

$$x_i(t) = X_i(t + 1) - X_i(t).$$

Then, since the algorithm is meant for the processing of physically nonuniform or, at least, different-scale uniform information, we calculate the sample mean s_i and

sample variance σ_i for each scalar component $x_i(t)$ and in each time window, normalizing to the unit variance

$$x_i(t) := (x_i(t) - s_i)/\sigma_i. \tag{1}$$

This operation permits the processing of physically heterogeneous and different-scale data.

To estimate the spectrum matrix of the multidimensional series $\mathbf{x}(t) = (x_1(t), \dots, x_m(t))^T$ in each time window, we apply the model of multidimensional autoregression

$$\mathbf{x}(t) + \sum_{k=1}^p A_k \mathbf{x}(t-k) = \boldsymbol{\epsilon}(t), \tag{2}$$

where A_k is the $(m \times m)$ matrix of the autoregression parameters, $p \geq 1$ is the order of autoregression, $\boldsymbol{\epsilon}(t)$ is the sequence of the Gaussian independent m -dimensional random vectors with zero mean and covariance matrix P . The matrices A_k , $k = 1, \dots, p$, and P were determined by the Darbin–Levinson method [14], which requires the preliminary determination of the covariance matrix $R_k = \langle \mathbf{x}(t)\mathbf{x}^T(t-k) \rangle$, $k = 0, 1, \dots, p$, where $\langle \dots \rangle$ is the sign of averaging over time.

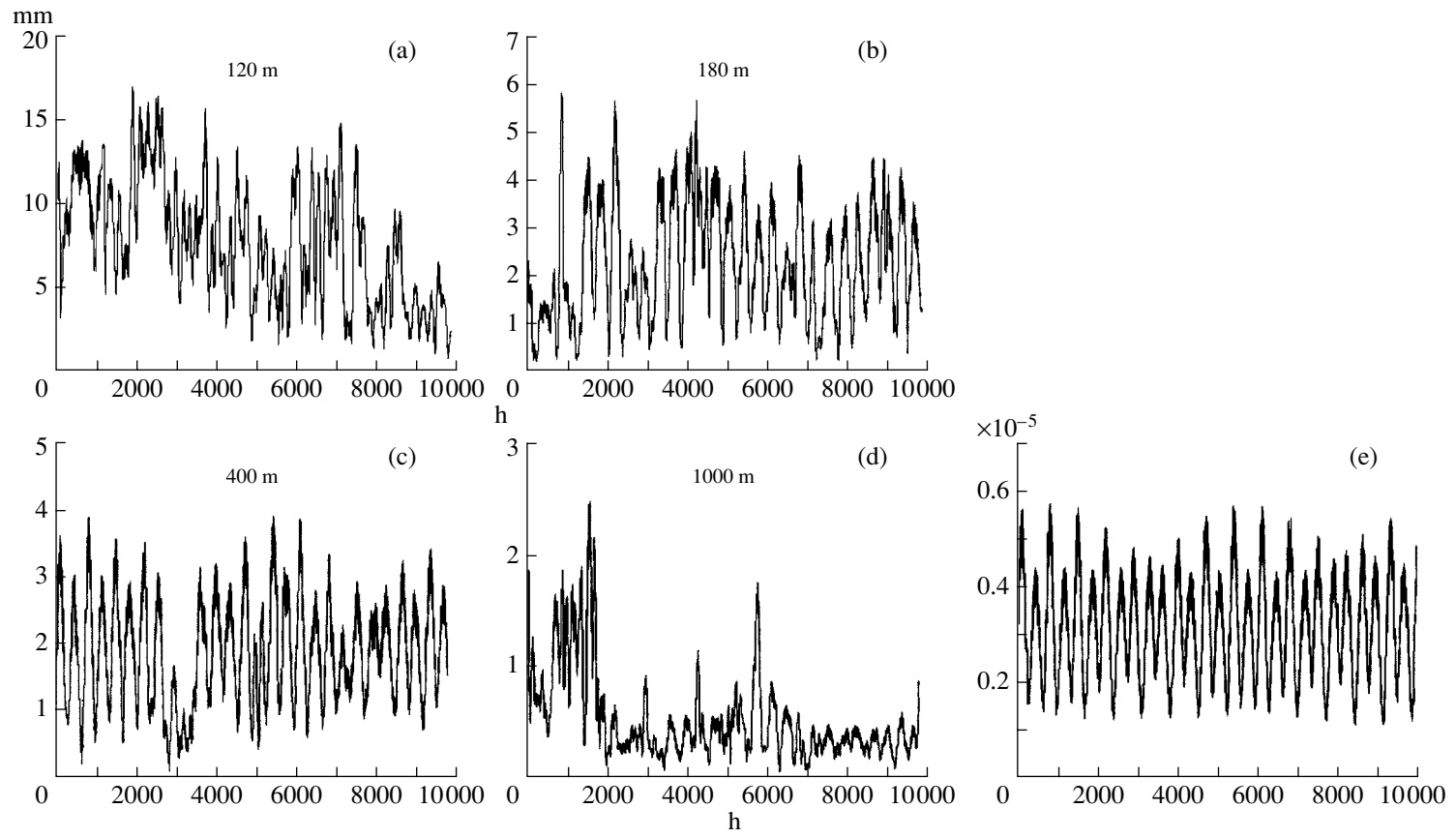


Fig. 3. Variations in variance of the compensated levels (a–d) and theoretical tidal volume deformations (e) in the 12-h tidal frequency band, calculated in the 48-h moving time window.

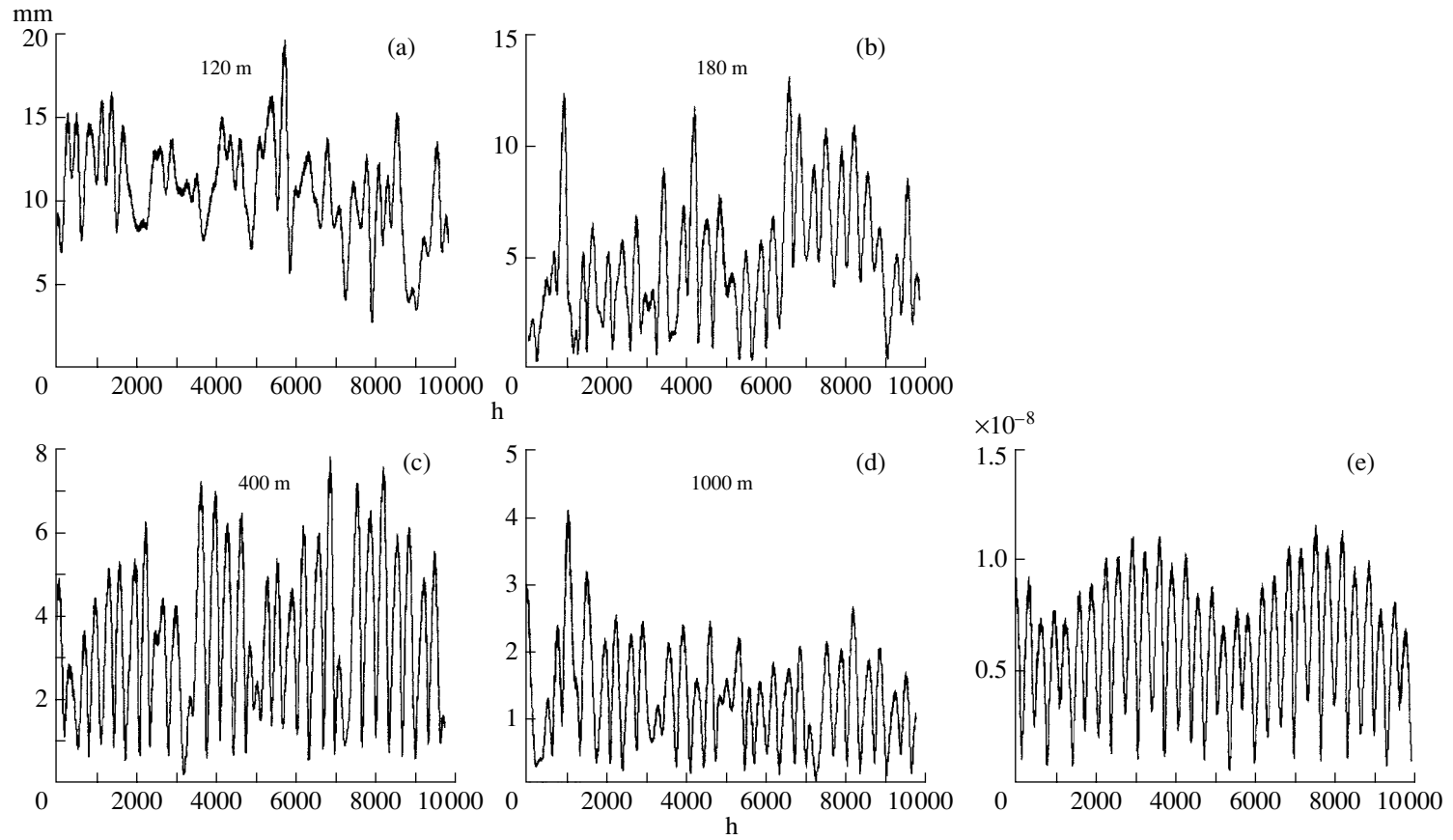


Fig. 4. Variations in the variance of the compensated levels (a–d) and theoretical tidal volume deformations (e) in the 24-h tidal frequency band, calculated in the 48-h moving time window.

After the determination of the matrices A_k and P , the spectrum matrix $S(\omega)$ is estimated

$$S^{-1}(\omega) = A^H(\omega)P^{-1}A(\omega),$$

$$A(\omega) = I + \sum_{k=1}^p A_k e^{-i\omega k}, \quad (3)$$

where I is the unit ($m \times m$) matrix, ω is the frequency, i is an imaginary unit, and H indicates the Hermitian conjugate matrix.

By definition (and according to the estimation algorithm), the spectrum matrix $S(\omega)$ is the Hermitian and nonnegatively definite. Therefore, its eigenvalues $\lambda_i(\omega)$, $i = 1, \dots, m$ are real and not negative. Ordering the eigenvalues by their decrease, we have

$$0 \leq \lambda_m(\omega) \leq \dots \leq \lambda_1(\omega). \quad (4)$$

According to the spectrum method of the principal components, the maximum eigenvalue $\lambda_1(\omega)$ is the power spectrum of a scalar series of the time series (series of the principal components) that is obtained from the initial vector time series $\mathbf{x}(t)$ by linear filtration and that bears the most information (for the Gaussian time series) on the behavior of the scalar components $x_i(t)$ of the initial series [13]. Thus, going from $S(\omega)$ to $\lambda_1(\omega)$, we maximally diminish the dimension (from m to 1) retaining the maximum information.

Since the spectrum matrix is estimated in the moving time window, the matrix and its eigenvalues depend on the time coordinate of the window τ , in addition to the frequency ω . For definiteness, we set τ equal to the time of the middle of the window. Then, the two-parametric function $\lambda_1(\tau, \omega)$ is plotted either by level lines or three-dimensional surfaces [12]. Our purpose is to construct and analyze $\lambda_1(\tau, \omega)$, i.e., diagrams for the multidimensional series of variance in the four holes.

Note that the model of multidimensional autoregression (2) may be used for the partial case $m = 2$ (for two-dimensional series) to estimate the evolution of the coherence spectrum modulus squared. For this, after estimating spectrum matrix (3), one must calculate it from the formula [13, 14]

$$\gamma^2(\omega) = |S_{12}(\omega)|^2 / (S_{11}(\omega)S_{22}(\omega)). \quad (5)$$

Similarly, being estimated in the moving time window, γ^2 becomes a function of two arguments $\gamma^2 = \gamma^2(\tau, \omega)$. This is the same approach that we used to estimate the evolution of γ^2 in comparing the levels with the theoretical tidal volume deformations. The comparison of the parametric estimates of γ^2 with the nonparametric (through the Fourier transformation and averaging periodograms [13]) showed their agreement, but the variance of the parametric estimates is 1.5–2 times lower.

RESULTS OF PROCESSING

Figures 5–8 show the results obtained for the series processed. Evolution of the square of the spectrum modulus of coherence γ^2 between each of the compensated levels and theoretical tidal deformation is presented in Figs. 5 and 6, and Figs. 7 and 8 illustrate different $\lambda_1(\tau, \omega)$ diagrams for the combined processing of several levels. For all the cases, the autoregression model (2) of the 15th order ($p = 15$) for dimensions of $m = 2, 3, 4$ was used. The size of the moving time window was 500 h, and the relative displacement of the windows was 100 h.

Consider Figs. 5 and 6. Naturally, only two frequency bands corresponding to 12- and 24-h tides are important for $\gamma^2(\tau, \omega)$, and for the other frequencies, $\gamma^2(\tau, \omega) \approx 0$. Therefore, diagrams of $\gamma^2(\tau, \omega)$ are depicted as so-called 12- and 24-h crests. We determine the narrow-band crest as a function of the time τ of the window

$$g(\tau) = \max_{\omega} \gamma^2(\tau, \omega), \quad \omega_{\min} \leq \omega \leq \omega_{\max}, \quad (6)$$

where the frequency bands $[1/13, 1/11] \text{ h}^{-1}$ and $[1/27, 1/23] \text{ h}^{-1}$ correspond to the 12-h (Fig. 5) in (6) and 24-h (Fig. 6) crests, respectively.

Figure 5a demonstrates the chaotic behavior of γ^2 near the mean value of about 0.4 with a significant variance. This suggests that the 12-h tidal variations of level 120 agree with the theoretical deformations, and this may well be explained by the effect of water supply from this horizon.

As to the other levels (Figs. 5b–5d), the evolution of γ^2 in the 12-h tidal band shows, in general, smooth behavior with an extended “plateau” approaching the constant value $\gamma^2 \approx 1$ (in good agreement with theory), with some drops in γ^2 (sometimes to $\gamma^2 \approx 0$) being represented as well. Each of the drops may be interpreted either as a local anomaly of the response of a water-bearing horizon to tides or as a time interval of increase in the power of the other signals (for example, anthropogenic). To separate these two causes by processing only one of the levels is not possible. Note that Fig. 5c reflects the anomalies revealed by us above in Fig. 3c relative to the “standard” behavior of the graph in Fig. 3e. By comparing the anomalies of γ^2 in Figs. 5b–5d, we may distinguish the general (in particular, near $t \approx 3000$ h) and specific anomalies only for the horizon considered (for example, two drops of γ^2 almost to zero (Fig. 5b), in the vicinity of $t \approx 900$ and 9000 h, in March 1993 and March 1994).

Figure 6 shows the 24-h crests of evolution of γ^2 between the levels and theoretical deformations. It is remarkable that the graphs in Fig. 6 often demonstrate completely different behavior from that in Fig. 5. For example, the 24-h tidal variations in level 120 are much closer to the theoretical tidal deformation (Fig. 6a) than the 12-h (Fig. 5a). This is explained by weaker anthropogenic noise for horizon 120 in the 24-h tidal band,

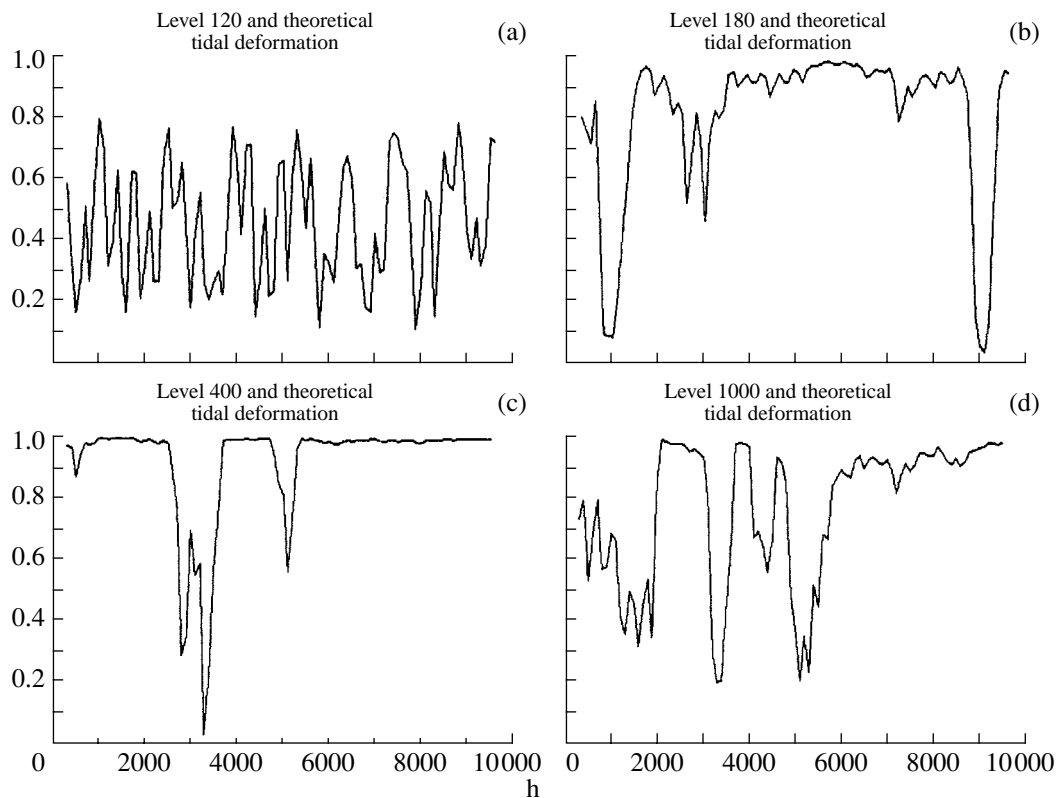


Fig. 5. Variations in the square of the modulus of the spectrum of coherence between the compensated levels and theoretical tidal volume deformations near 12 h.

compared with the 12-h band. The closest similarity between the 12- and 24-h crests is observed for horizon 400 (Figs. 5c, 6c). Furthermore, in complete agreement with the previous, visually noted anomalies in Fig. 4c (compared with Fig. 4e), an additional anomaly of γ^2 appeared near $t \approx 7000$ h (Fig. 6c). Comparison of Figs. 6b and 5b shows both agreement and disagreement of the 12-h (Fig. 5b) and 24-h (Fig. 6b) tidal components of level 180 with the theoretical deformations for $t < 5500$ h; the 24-h variations in level 180 are totally at variance with theory (Fig. 6b), unlike the 12-h variations (Fig. 5b), which show relatively narrow intervals of disagreement. However, for $t > 5500$ h, γ^2 for the 12- and 24-h variations in level 180 is consistent up to the appearance of a deep and synchronous drop in γ^2 near $t \approx 9000$ h. Comparison of Figs. 6d and 5d (level 1000) also suggests that the time anomalies (disagreement between tidal variations in the level and theoretical deformations) are of "local" character not only relative to the given horizon but also relative to the frequency band for the same level.

Thus, from Figs. 5 and 6, one can see the difficulties of revealing the general causes and trends in the analysis of complex (multidimensional) geophysical time series in the case when processing is not multidimensional. Each of the anomalies of γ^2 in Figs. 5 and 6 reveals a specific feature of the response of a water-bearing horizon to tides. The feature may be both of

geophysical (change in properties of the horizon) and anthropogenic character (change in the regime of water supply). The causes of these features may be local (inherent in a horizon) or regional (common to all the horizons examined). Naturally, most interesting is the identification of regional anomalies, since they are most likely to be related to natural geophysical processes, whereas the anthropogenic causes (in our case, water supply from levels 120 and 180) are always local. The frequency-time method of the principal components is intended namely to reveal the general causes in data of geophysical monitoring and remove local noises [11, 12].

Figure 7 presents the $\lambda_1(\tau, \omega)$ diagrams (evolution of the first eigenvalue) of the four-dimensional spectrum matrix for the levels compensated for the effect of atmospheric pressure (Fig. 7a) and, for comparison, for the initial levels (Fig. 7b). The given frequency range is 0.01 to $1/5$ h^{-1} , since there are no specific features for periods shorter than 6 h. In Fig. 7a, one can see two frequency bands, in which the compensated levels synchronously vary in the vicinity of frequencies of $1/12$ and $1/24$ h^{-1} . The synchronization is not observed in the other frequency bands, including low-frequency. A totally different picture is seen in Fig. 7b ($\lambda_1(\tau, \omega)$ for the initial levels). Here, the vicinity of the frequency of $1/12$ h^{-1} is also identified, but the 24-h crest is completely suppressed by signals of the low-frequency syn-

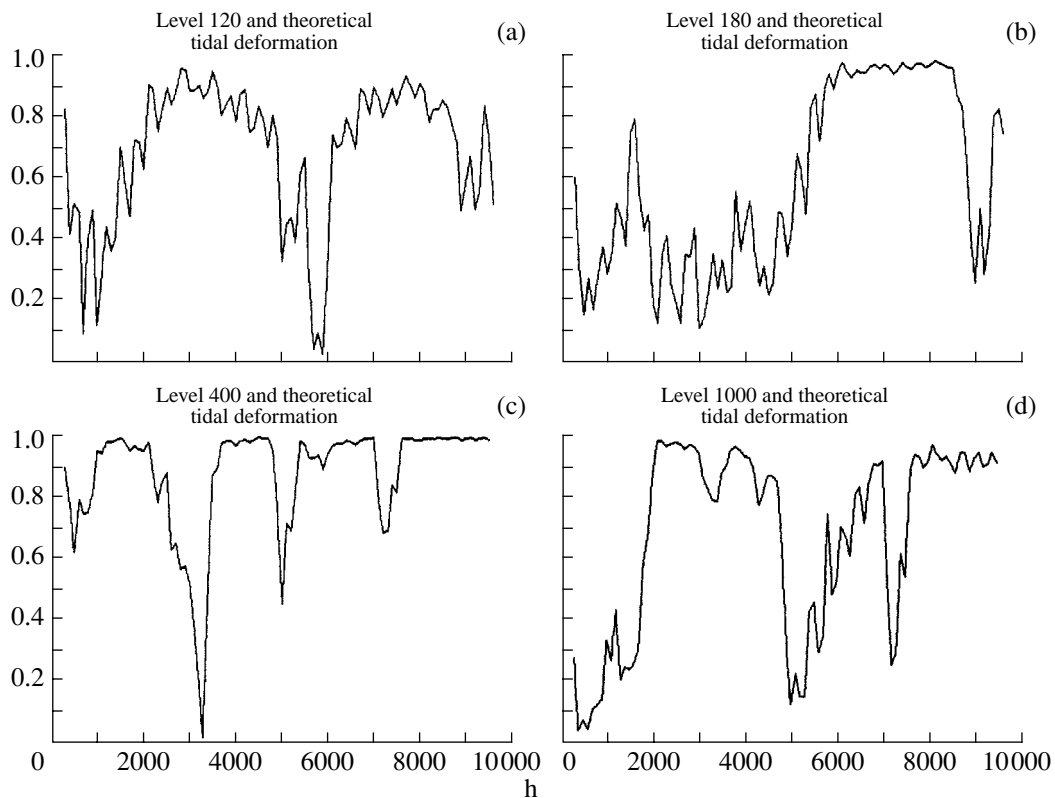


Fig. 6. Variations in the square of the modulus of the spectrum of coherence between the compensated and theoretical tidal volume deformations near 24 h.

chronization that are caused by the same external low-frequency baric variation acting upon all four levels. This example demonstrates the importance of the preliminary compensation of noises.

Figure 8 shows the 12- and 24-h crests (according to (6)) of the evolution of the first eigenvalue for the four-dimensional spectrum matrix of all the compensated levels (Figs. 8a, 8e, solid line) and for all the variants of the three-dimensional matrix, when one of the levels is sequentially removed from the four levels analyzed (Figs. 8a, 8e and others, broken lines). Figure 8 also shows the identifiers of the levels corresponding to the depths of occurrence of water-bearing horizons.

Let us turn to the 12-h crest of evolution of λ_1 for the matrix of all four compensated levels (Fig. 8a, solid line). Characteristic for it is the stable recurrence of some specific features, for example “double teeth” for $t = 1800\text{--}2200$, $3800\text{--}4200$, $5800\text{--}6200$, and $8400\text{--}8800$ h. For $t = 3600\text{--}6400$ h, the graph forms a symmetrical (relative to $t \approx 5000$ h) structure of the duration of about half a year. In general, the 14-h (distance between the “small teeth”) and almost semiannual periodicities are inherent in the graph.

Now we sequentially remove one of the four levels at a time and, for the remaining levels, plot the evolution of λ_1 for the 12-h crest (Fig. 8a, broken line; Figs. 8b–8d). All the specific features seen in Fig. 8a (solid line) are found to be retained (with small alter-

ations mainly in the amplitude of variations in λ_1 , but not in their shape), where level 400 is present (Figs. 8b–8d). Variations of λ_1 near the frequency of $1/12 \text{ h}^{-1}$ for the 3×3 matrix of the horizons 120, 180, and 1000 (Fig. 8a, broken line) are totally different: the general level of values of λ_1 is significantly lower (suggesting weaker synchronization), and the regular long-period structures seen in the other figures are absent, while the 14-h periodicity is retained. Thus, for the 12-h crest, level 400 may be called “leading” in the sense that it maximally accumulates the 12-h tidal variations common to all the horizons.

The general level of λ_1 of the 24-h crest is lower than that of the 12-h crest, and the semidiurnal structure is absent for the former. Here, horizon 400 may also be called “leading,” since, if it is not involved in processing, (Fig. 8e, broken line), the general synchronization level (value of λ_1) is smallest. For $t = 6000\text{--}9000$ h, a splash in the λ_1 values for the four-dimensional matrix (Fig. 8e, solid line) is observed; when horizon 180 is involved in processing apart from level 400, the splash repeats (Figs. 8f, 8h), preserving the amplitude and shape to a marked extent. Thus, horizon 180, in addition to horizon 400, is secondary in importance for the 24-h tidal variations in the levels. As to the 14-h periodicity, it is also presented in graphs of the 24-h crest but is more weakly pronounced than that of the 12-h crest.

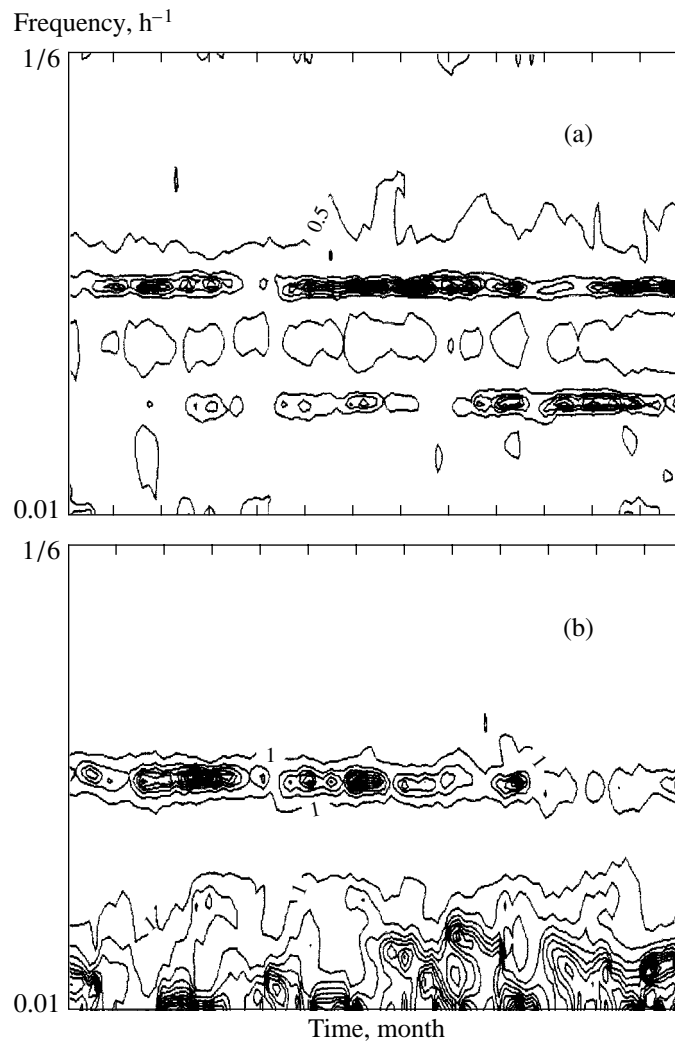


Fig. 7. Evolution of the maximum eigenvalue of the spectrum matrix of the four-dimensional time series of the (a) compensated and (b) initial levels.

INTERPRETATION

Our purpose was to estimate the time variability of both the response of horizons to tides (Figs. 5, 6) and the similarity (synchronism) of variations in the response for several horizons (Figs. 7, 8). Let us represent variations in the underground water levels in holes as a set of local signals inherent in a given horizon, regional signals common to all the water-bearing layers in the area examined, and global signals such as tidal deformations in the crust. This division is conditional and not based on any laws of dynamics of underground water, but on simple cause-effect relations. The specific features of a water-bearing horizon determine the proportion of the local, regional, and global signals in the measured level. For example, if the thickness of the water-bearing horizon is small, its structure is discontinuous and lenslike, and, as a result, it possesses small water conductivity, then the fraction of the local signals in the measured level will be small, since the propaga-

tion of signals in the water-bearing horizon from other regions is accompanied by strong attenuation and lagging. Conversely, a horizon having a high piezoelectric conductivity is able to transfer signals without substantial attenuation; then, weakly correlated local signals, being summed, are averaged and produce a total effect close to zero. Thus, a water-bearing horizon of high conductivity is something of a spatial filter emphasizing regional signals and suppressing local ones.

From the aforesaid, it becomes clear why horizon 400 plays the leading role in the combined analysis of time series of level variations, since its thickness is substantially greater than that of the other horizons (see table). Variations in level 400 initially have a small level of local noises, including anthropogenic noise (this level is not used for industrial water supply). Hence, it follows that level 400 agrees most closely with the theoretical volume tidal deformations (Figs. 5c, 6c).

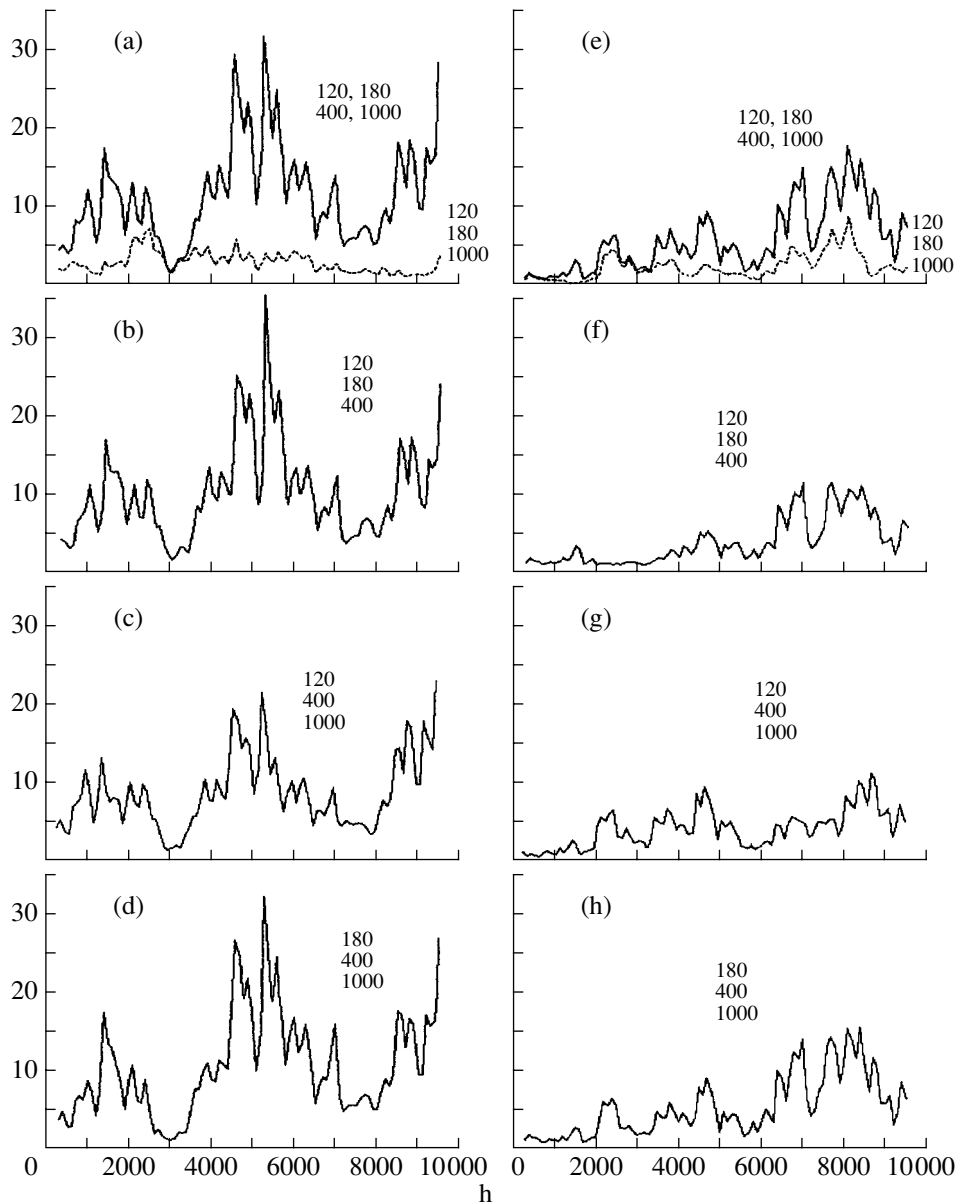


Fig. 8. Evolution of the maximum eigenvalue of the spectrum matrix in different variants of combined processing of compensated level series near 12 h (a, b, d, e) and 24 h (e-h).

The thickness of horizon 1000 is also significant, but propagation of signals in it is likely to be impeded by its lenslike structure (table). In particular, the increase in the amplitude of high-frequency variations in level 1000 for $t = 500-1700$ h (Fig. 3d) may be produced by the closer contact between the lenses. In spite of its small thickness, the conductivity of horizon 120 is high [9], but variations in its level contain many anthropogenic noises (water supply effect). Horizon 180 possesses a relatively low thickness and conductivity, and the water supply from it is much lower than that from horizon 120. This apparently determines the fact that horizon 180 was found to be in second place after

horizon 400 in saturation with general (regional) signals.

In the combined processing of a few levels by the spectrum method of the principal components, local signals (as noise) are suppressed, and regional and global signals are identified. However, the effect of this multidimensional filtration is obviously determined by the signal-to-noise ratio, which is largest for the variants in Figs. 8b, 8d, 8f, and 8h and smallest for the variant (120, 180, and 1000) shown by broken lines in Figs. 8a and 8e.

Thus, the method described above allows us to compare the importance of water-bearing horizons in the identification of regional signals.

Differences between the curves in Figs. 5, 6, and 8 for various frequency bands suggest that the responses of water-bearing horizons to an external action with periods of 12 and 24 h will be substantially different. This is confirmed by estimates of the transfer function of baric variations [1]. However, we did not expect that the degree of synchronization for the 24-h tidal variations in the levels would be 2 times smaller than that for the 12-h variations. This may be due to some specific features of the leading horizon 400. Furthermore, it was not also expected that splashes of synchronization for the 12-h variations would not coincide with those for the 24-h variations.

The presence of the 14-h and semidiurnal (for the 12-h crest) periodicities in the evolution of synchronization (Fig. 8) may be caused by the effect of the 14-h and semidiurnal modulations of tides (Figs. 3e, 4e) on the strength of the upper crust (on the force of cohesion between crustal blocks). When the amplitude of the total volume deformation (i.e., the sum of the 12- and 24-h components) is smallest, the crustal blocks are weaker relative to each other than when the amplitude of the tides is largest.

CONCLUSION

We have developed a method for the combined analysis of tidal variations in the levels of a set of holes drilled down to different water-bearing horizons. The method enables one to identify the time intervals in which the tidal variations of the levels correspond to theoretically derived tidal volume deformations; moreover, the method estimates the change in time of the combined synchronization of the tidal variations in the levels for the entire set of horizons.

The method is applicable to the processing of synchronous observations of the levels in the four holes drilled in the Moscow region. Results of processing showed that the agreement between the tidal variations in the levels and theoretical tidal deformations ($\gamma^2(\tau, \omega)$, including the horizons not used for water supply) is substantially unstable, like the degree of synchronization of the tidal variations in the levels ($\lambda_1(\tau, \omega)$). Furthermore, the character of evolution of the parameters estimated for the 12- and 24-h tidal frequency bands is different.

The 14-h diurnal and semiannual periodicities were established in the evolution of the joint synchronization of the 12-h tidal variations. The periodicities may be the result of the effect of the 14-day and semiannual variations in the amplitude of tidal variations on the strength of the upper crust.

The method developed enabled us to identify the most significant water-bearing horizons, for which

variations in the levels are the most saturated with general (regional) signals. This may be useful for choosing observed horizons and planning monitoring in seismic zones.

ACKNOWLEDGMENTS

This work was supported by the Russian Foundation for Basic Research, grant no. 94-05-16120.

REFERENCES

1. Lyubushin, A.A. and Malugin, V.A., Statistical Analysis of the Response of Underground Water to Variations in the Atmospheric Pressure, *Fiz. Zemli*, 1993, no. 12, pp. 74–80.
2. Melchior, P., *The Earth Tides*, New York: Pergamon, 1966.
3. Bredehoft, J.D., Response of a Well-Aquifer System to Earth Tides, *J. Geophys. Res.*, 1967, vol. 12, pp. 3075–3087.
4. Igarashi, G. and Wakita, H., Tidal Response and Earthquake-related Changes in the Water Level of Deep Wells, *J. Geophys. Res.*, 1991, vol. 96, pp. 4269–4278.
5. Rojstaczer, S. and Agnew, D.C., The Influence of Formation Material Properties on the Response of Water Levels in Wells to Earth Tides and Atmospheric Loading, *J. Geophys. Res.*, 1989, vol. 94, pp. 12403–12411.
6. Bagmet, A.L., Bagmet, M.I., Barabanov, V.L., et al., Study of Tidal Oscillations of the Underground Water Level in the Obninsk Well, *Izv. Akad. Nauk SSSR, Fiz. Zemli*, 1989, no. 11, pp. 84–95.
7. Sardarov, S.S. and Alibekov, B.I., Periodic Concentration of He in Natural Gas, *Izv. Akad. Nauk SSSR, Fiz. Zemli*, 1977, no. 9, pp. 102–106.
8. Kissin, I.G. and Gumen, A.M., Hydrogeological Indicators for Recent Movements of the Crust in an Aseismic Region, *Dokl. Ross. Akad. Nauk*, 1994, vol. 334, no. 6, pp. 768–772.
9. *Gidrogeologiya SSSR* (Hydrogeology of the Soviet Union), Moscow: Nauka, 1966, vol. 1.
10. Lyubushin, A.A. and Latyninas, L.A., Compensation of Meteorological Noise in Strainmeter Measurements, *Fiz. Zemli*, 1993, no. 3, pp. 98–102.
11. Lyubushin, A.A., Multidimensional Analysis of Time Series from Geophysical Monitoring, *Fiz. Zemli*, 1993, no. 3, pp. 103–108.
12. Lyubushin, A.A. Classification of States of Low-Frequency Geophysical Monitoring, *Fiz. Zemli*, 1994, no. 7, pp. 135–141.
13. Brillinger, D., *Time Series. Data Analysis and Theory*, New York: Holt, Rineheart, and Winston, 1975. Translated under the title *Vremennyye ryady. Obrabotka dannykh i teoriya*, Moscow: Mir, 1980.
14. Marpl, S.L., *Tsifrovoy spektral'nyi analiz i ego prilozheniya* (Digital Spectral Analysis and Its Application), Moscow: Mir, 1990.